OPEN ACCESS
IOP Publishing
Classical and Quantum Gravity
Class. Quantum Grav. **41** (2024) 175016 (13pp) https://doi.org/10.1088/1361-6382/ad672c

Monitoring the evolution of optical coatings during thermal annealing with real-time, *in situ* spectroscopic ellipsometry

Stefano Colace[1], Shima Samandari[1], Massimo Granata[2], Alex Amato[3], Michael Caminale[1], Christophe Michel[2], Gianluca Gemme[4], Laurent Pinard[2], Maurizio Canepa[1,*] and Michele Magnozzi[1,4,*]

[1] OptMatLab, Dipartimento di Fisica, Università di Genova, via Dodecaneso 33, 16146 Genova, Italy
[2] Laboratoire des Matériaux Avancés—IP2I, CNRS, Université de Lyon, Université Claude Bernard Lyon 1, F-69622 Villeurbanne, France
[3] Maastricht University, PO Box 616, 6200 MD Maastricht, The Netherlands
[4] Istituto Nazionale di Fisica Nucleare, Sezione di Genova, via Dodecaneso 33, 16146 Genova, Italy

E-mail: canepa@fisica.unige.it and magnozzi@fisica.unige.it

Received 21 December 2023; revised 27 May 2024
Accepted for publication 24 July 2024
Published 8 August 2024

Abstract

Thermal annealing plays a key role in optimizing the properties of amorphous optical coatings. In the field of gravitational wave detection (GWD), however, the effects of annealing protocols on the interferometry mirror coatings have been explored primarily by *ex post* analysis. As a result, the dynamics of the coatings properties during annealing is still poorly known, potentially leading to suboptimal performance. Here, using real-time, *in situ* spectroscopic ellipsometry (SE) we have tracked the refractive index and thickness of a titania-tantala coating during controlled annealing. We have tested the material and the annealing protocol used in current GWD mirrors. The annealing cycle consisted of a heating ramp from room temperature to 500 °C, followed by a 10-h plateau at the same temperature and the final cooling ramp. SE measurements have been run continuously during the entire cycle. Significant variations in the thickness and refractive index, which accompany the coating

* Authors to whom any correspondence should be addressed.

structural relaxation, have been recorded during the heating ramp. These variations start around 200 °C, slightly above the deposition temperature, and show an increased rate in the range 250 °C–350 °C. A smaller, continuous evolution has been observed during the 10-h high-temperature plateau. The results offer suggestions to modify the current annealing protocol for titania-tantala coatings, for example by increasing the time duration of the high-temperature plateau. They also suggest an increase in the substrate temperature at deposition. The approach presented here paves the way for systematic, real-time investigations to clarify how the annealing parameters shape the properties of optical coatings, and can be leveraged to define and optimize the annealing protocol of new candidate materials for GWD mirrors.

Keywords: thermal annealing, spectroscopic ellipsometry, optical coatings, real-time, GWD mirrors

1. Introduction

Thermal annealing is a process commonly used to enhance the performance of amorphous optical coatings [1–3]. It can increase the transmittance [4] and stability [5], and reduce the absorptance [6] and the stress which might result from optical coatings deposition [7, 8]. For these reasons, thermal annealing is mandatory for high-performance amorphous coatings, such as the ones used as mirrors in gravitational wave detectors (GWD) [9–12]. Thermal annealing is defined by a few parameters, such as the heating rate, the maximum temperature, the time spent at the maximum temperature, and the cooling rate. Finding the optimal annealing parameters for an optical coating in GWD applications is no easy task. For instance, one has to balance the advantages of a high-temperature annealing with the risk of inducing undesired crystallization, which must be avoided in mirror coatings for GWD applications [10, 13].

The search for the optimal annealing parameters is often based on *ex-post* analysis, which in this context means to probe the coating before and after the annealing [14–19]. Within the GWD community, educated trial-and-error procedures and *ex-post* analysis [11] have guided the definition of a standard annealing protocol for the amorphous mirror coatings. But since no information was recorded about the evolution of coatings properties during the annealing, such protocol might not be based on optimal parameters.

On the other hand, a real-time monitoring of the annealing would clarify the dynamics of the key coatings properties [20–22] as a function of annealing time and temperature. Moreover, it would provide experimental data to support theories about the temperature-induced relaxation in amorphous materials, and would help to understand threshold effects such as blistering or delamination [23]. Indeed, real-time monitoring of the annealing is a powerful tool to facilitate the optimization of the annealing parameters for optical coatings.

In this work, we present a real-time, *in situ* monitoring of the thermal annealing of an amorphous TiO_2:Ta_2O_5 (titania-tantala) coating by means of spectroscopic ellipsometry (SE). Titania-tantala is employed as the high-index material used in current GWD mirror coatings, which consist of alternating layers of amorphous SiO_2 and TiO_2:Ta_2O_5 fabricated by means of ion beam sputtering (IBS) [11, 24, 25]. Enhancing the properties of the high-index layer would positively affect the performance of the whole mirrors [26], and the optimization of the annealing process is a valuable tool to this end. SE is a powerful technique to study optical coatings and monitor in real time the evolution of optical properties during thermal processes

on a variety of thin and ultrathin films due to its high sensitivity to parameters such as thickness, refractive index, and morphology [27–32].In this investigation we elected to test the annealing protocol that has been used on current GWD mirrors. By means of real-time, *in situ* SE, we track the optical response of a titania-tantala coating during the whole annealing process in a wide spectral range, determining the evolution of its refractive index and thickness as a function of temperature and annealing time. By providing access to the dynamics of optical coatings properties during the annealing, the method proposed in this paper can be applied to tune the annealing parameters of amorphous titania-tantala coatings, or of any other coating for GWD applications. It can even provide useful feedback on the choice of growth parameters, such as the substrate temperature at deposition.

2. Materials and methods

2.1. Materials

The optical coating considered in this work consists of a thin layer of nominal thickness equal to 475 nm, made of amorphous titania-doped tantala. The nominal cation ratio is Ti/(Ta+Ti) $= 25\%$, the same used in the actual GWD mirrors. The coating was deposited by IBS at the Laboratoire des Matériaux Avancés (http://lma.in2p3.fr/) using a custom made coater machine (Grand Coater), developed to deposit the large high-reflective mirrors for GWDs [10, 33]. During the deposition, the substrate temperature was approximately 150 °C.

The coating was deposited on a single-side polished Silicon wafer manufactured by Siltronix with the following characteristics: P-doped, resistivity ρ: <1 Ω·cm, orientation: (100)+/−0.5°, nominal thickness: 0.5 mm. In the context of the SE measurements and data analysis of this work, single-side polished Si is perhaps the best substrate because it guarantees a high optical contrast with respect to the titania-tantala coating [34], together with the absence of unwanted backside reflections [35].

2.2. Experimental methods

A scheme of the experimental setup for real-time ellipsometry during thermal annealing is shown in figure 1. The sample was annealed using a Linkam THMS600 temperature controlled stage, which allows heating up to 600 °C with stability better than 0.01 °C. The heating element of the THMS600 cell is composed of a pure silver cylinder crossed by a heating wire. Temperature is read on the side of the cylinder by means of a Pt sensor. The lateral size of the sample was 1×1 cm^2. The stage is equipped with a top cover with two windows for ellipsometric access, which set the SE angle of incidence to 70°. The windows do not alter the polarization state of the incident light, an important aspect that was verified before acquiring the measurements reported in this work [27]. Thermal annealing was performed in air, following the standard post-deposition protocol for GWD coatings produced by LMA, that is, a heating ramp at 100 °C h^{-1} up to 500 °C followed by a 10-h plateau at 500 °C and finally a cooling ramp at 100 °C h^{-1} [9, 11, 36].

SE data were acquired using a J A Woollam Co., Inc. M2000 ellipsometer. Spectral range was between 0.7 and 5.1 eV (245–1685 nm, 0.18–1.22 $\times 10^{15}$ Hz). The beam diameter was approximately 4 mm. SE data were analyzed with WVASE software by J A Woollam Co., Inc.. SE data were acquired during the whole annealing process. The acquisition time for a single SE spectrum was below 3 s.

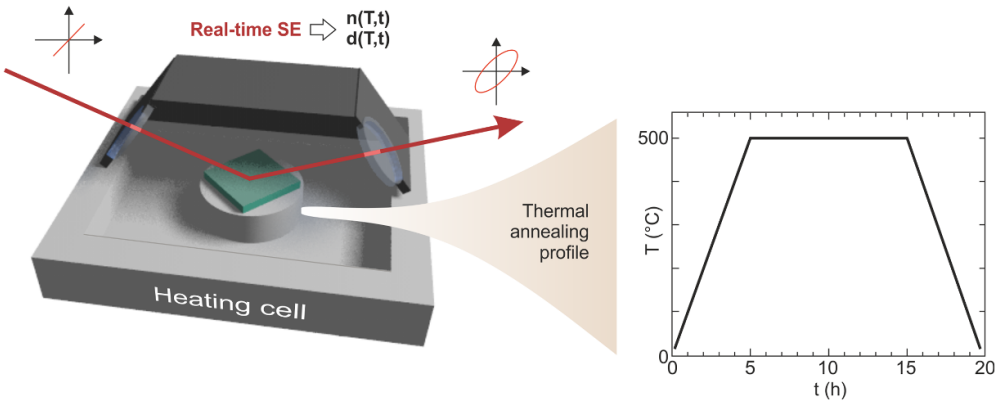

Figure 1. Scheme of the experimental setup. The titania-tantala coating, deposited on a $1 \times 1\,\mathrm{cm}^2$ silicon wafer, is placed on top of a cylindrical heater, whose temperature varies between 20 and 500 °C. The heater stage has a top cover equipped with windows, thus allowing the SE beam (red line) to probe the sample in real time during the thermal annealing. To allow a clear view of the inner part of the heating cell, the top cover has been cut in half in the scheme. Analysis of real-time SE data yields the temperature- and time-dependent refractive index n(T,t) and thickness d(T,t) of the coating. The panel on the right describes the annealing protocol used in this work: from left to right, the three segments correspond to the heating ramp, the high-temperature plateau, and the cooling ramp. The coating material and the annealing protocol in this work match those employed in current GWD mirrors.

SE spectra consist of two values, conventionally labeled Ψ and Δ, which are related to the complex Fresnel coefficients r_p, r_s of the sample under investigation: $\Psi = \arctan(|r_p|/|r_s|)$ and $\Delta = \delta_p - \delta_s$, where $|r_{p,s}|$ and $\delta_{p,s}$ are the modulus and the phase of $r_{p,s}$, respectively [37]. The nature of Ψ and Δ implies that SE measurements do not need any reference beam, thus making SE a particularly well suited tool for real-time, *in situ* investigations where the temperature of the sample is varied [27, 28, 31, 38, 39]. The quantities of interest, such as the refractive index and thickness of a coating, are extracted from Ψ, Δ by means of a model-based data analysis [37].

Before and after the annealing, the sample was characterized by AFM and Raman spectroscopy to evaluate possible variations induced in the surface and structural properties by annealing. AFM images were acquired with a Veeco Dimension 3100 instrument in tapping mode and processed with the open-source software Gwyddion [40]. Raman spectroscopy was performed by means of a Jasco NRS-4100 confocal Raman spectrometer with excitation source at $\lambda = 532$ nm focused to a $\sim 1\ \mu$m spot size using a $100\times$, 0.9 NA objective.

The results of AFM and Raman investigation are reported in figure 2. AFM indicates a relatively low RMS roughness of 0.3 nm over a $10 \times 10\ \mu\mathrm{m}^2$ area (figure 2(a)), a value which does not significantly change when the size of the image is reduced to $1 \times 1\ \mu\mathrm{m}^2$ (figure 2(b)), and even more importantly, after the annealing (figures 2(b) and (c)). In this way, we determine that the surface quality of the sample has not been altered by the thermal treatment. Raman spectroscopy shows that no new peaks arise after the thermal annealing, thus indicating that the coating has remained amorphous throughout the process [29].

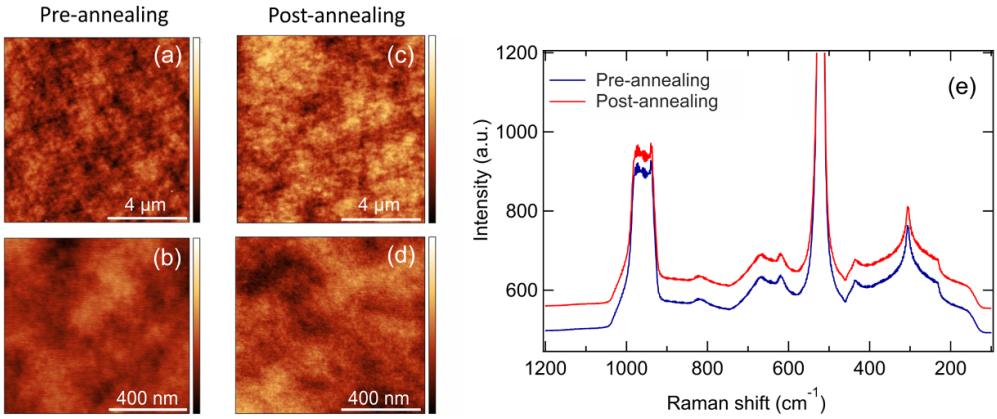

Figure 2. Panels (a), (b): AFM images pre-annealing; panels (c), (d): AFM images post-annealing). The color scale spans from 0 to 3 nm in panels (a), (c) and from 0 to 2 nm in panels (b), (d). Panel (e): Raman spectra pre- and post-annealing, which indicates that no crystallization peaks arise as a consequence of the annealing. The two spectra are vertically shifted for clarity.

3. Results and discussion

To study the evolution of the coating properties upon annealing it is first necessary to identify and isolate the contribution of the substrate on which the coating has been deposited. In this work silicon has been chosen as substrate because it is ideal for SE measurements and data analysis, however its optical response varies significantly with the temperature [41–45]. We determined the temperature-dependent optical properties of the silicon substrate by means of an independent measurement, where we performed a thermal annealing on silicon with the same parameters used for the titania-tantala coating sample, and recorded with real-time SE the evolution of its optical response.

The resulting SE data have been modeled by means of a multiparametric dispersion relation developed by J A Woollam Co., Inc. [46], whose parameters were tailored by us to match the optical properties of the Si used in this work. Figure 3 reports the temperature-dependent SE data (panels (a) and (b)) when heating the substrate from room temperature to 500 °C, as well as the refractive index (panel (c)) and extinction coefficient (panel (d)) obtained by means of SE data analysis. It is important to note that all the variations reported in figure 3 are reversible, meaning that the optical properties of Si are restored to the initial values once the annealing is over.

Once obtained the necessary information on the substrate, we performed real-time SE on the sample composed of titania-tantala coating on silicon during the heating ramp, the high-temperature plateau, and the cooling ramp. We report in figure 4 the Ψ spectra of the sample at four relevant steps of the annealing profile, namely, before the annealing, at the end of the heating ramp at 500 °C, at the end of the high-temperature plateau, and at the end of the cooling ramp. Difference spectra located below each panel in figure 4 highlight the magnitude and spectral position of differences between the corresponding Ψ spectra; in all cases, the difference is calculated by subtracting the first spectrum from the second spectrum in the graph legend. In figure 4(a) we compare the Ψ spectra before the annealing (grey curve) and at the end of the heating ramp (blue curve). Here, the difference between the two spectra are caused by irreversible variations in the titania-tantala coating as well as by reversible variations in the

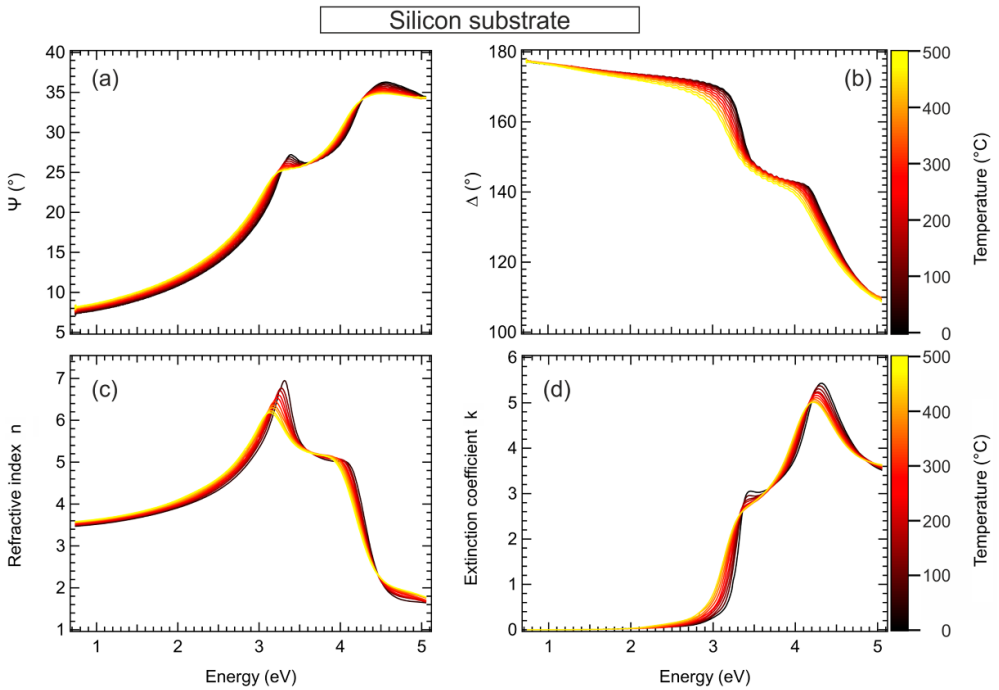

Figure 3. Temperature-dependent ellipsometry data (Ψ and Δ in panels (a) and (b), respectively), refractive index (panel (c)) and extinction coefficient (panel (d)) of the Si substrate determined from room temperature to 500 °C.

silicon substrate. In figure 4(b) we report the Ψ spectra of the sample upon reaching 500 °C (blue curve) and after 10 h at 500 °C (red curve). Since the temperature is constant in this case, the differences observed between the two spectra in figure 4(b) are exclusively due to the coating. Finally, in figure 4(c), we report the Ψ spectra of the sample before (grey curve) and after (green curve) the annealing. The data in this panel correspond to an *ex post* analysis. We can safely attribute the variations in figure 3(c) to permanent, annealing-induced modifications in the properties of the titania-tantala coating.

The Ψ data reported in figure 4 are characterized by broad oscillations in the spectral region up to ∼3.5 eV, followed by a smooth and featureless curve at higher energies. The broad oscillations are determined by interference effects in the titania-tantala coating, and indicate that the coating is transparent in that spectral region. Variations in the intensity and spectral position of these oscillations can be linked to variations in the refractive index and thickness of the coating by means of SE data analysis [34]. On the other hand, in the region where Ψ is smooth, the coating is absorbing. Since Ψ spectra can be so easily interpreted for this sample, we choose to show and discuss them in figure 4; similar considerations could be made on the Δ spectra. Both Ψ and Δ are necessary in order to extract the refractive index and thickness of the coating from SE data.

In this work we consider the refractive index at 1064 nm (1.17 eV), since this wavelength is currently used in GWD, and also at 1550 nm (0.80 eV), because future envisioned GWD might operate at that wavelength or anyway further in the near infrared (NIR) [47]. Thickness is best evaluated by considering the spectral region where the coating is transparent, which for titania-tantala is the NIR. We analyze the SE data in the NIR (1000–1685 nm) by modeling

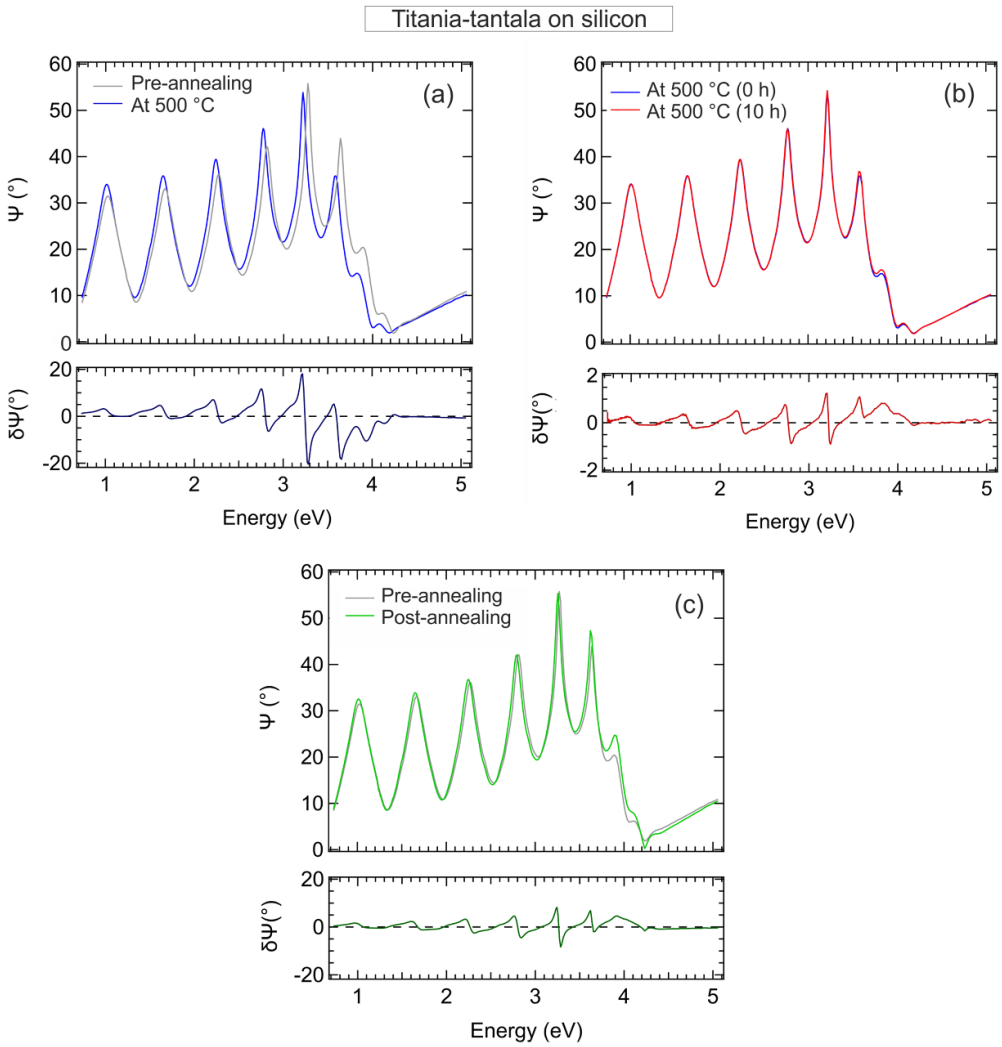

Figure 4. (a): Ψ pre-annealing and at 500 °C (grey and blue curve, respectively); (b) Ψ at 500 °C at the beginning and at the end of the high-temperature plateau (blue and red curve, respectively). (c): Ψ pre- and post-annealing (grey and green curve, respectively). Below each panel is reported the difference between the two corresponding Ψ spectra. Note that the scale of the difference spectrum in panel (b) is ten times smaller than those in panels (a) and (c).

the coating with a Cauchy layer, and modeling the substrate as detailed earlier. This model allows to decouple the reversible temperature-dependent variations in the substrate, already characterized in figure 3, from the irreversible temperature- and time-dependent variations in the coating, which constitute the main result of this work. To determine the Urbach energy, which will be discussed later, we adopted a Cody–Lorentz model across the whole available spectral range (245–1685 nm), following an approach described in previous works [48].

The results of the SE analysis are reported in figure 5. According to these data, the first substantial variations in the thickness and refractive index of the coating occur between 200 and

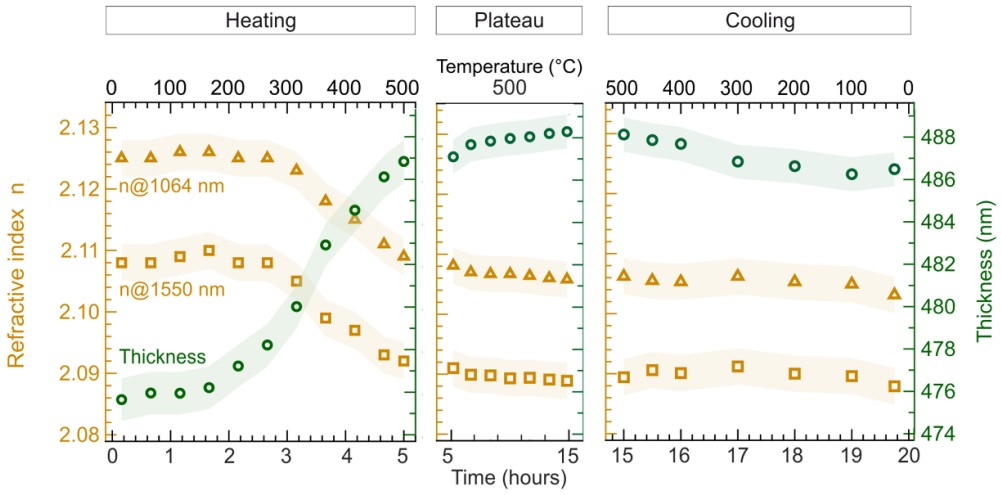

Figure 5. Refractive index (left axes) and thickness (right axes) of the titania-tantala thin film recorded during the heating (left panel), the 500 °C plateau (middle panel) and the cooling (right panel). The colored bands around points indicate the error bar.

300 °C in the heating ramp, while the maximum rate of variation is observed around 350 °C. After reaching the maximum temperature of 500 °C, the sample undergoes further yet smaller modifications during the 10 h plateau. Finally, the reduction in thickness as well as in the refractive index when cooling the sample from 500 °C is ascribed to the reversible temperature-induced effects on the titania-tantala coating [21, 49]. Overall, the thickness increases by $\sim$2.3%, while the refractive index decreases by $\sim$1%. In accordance with previous *ex-post* reports [14], the increase in thickness dominates, and as a result, the optical thickness of the coating is increased after annealing [48, 50, 51]—a feature that is potentially beneficial for GWD mirrors.

We attribute the observed variations to a complex interplay of physicochemical mechanisms intrinsically related to the release of compressive stress, which is caused the IBS deposition method [51, 52]. These mechanisms, which improve the optical and mechanical properties in amorphous transition metal oxides, can be best understood within an atomistic view on the coatings. The atomic structure of amorphous titania-tantala is composed of Ti-based and Ta-based oxygen-sharing polyhedra [53–55]. Polyhedra can be linked by a vertex, an edge or a face [56], and annealing can significantly affect the way in which polyhedra are interconnected. In particular, an increase in the corner-sharing to edge-sharing ratio has been observed in amorphous mixed zirconia-tantala films following annealing, along with variations in the Ta coordination number and variations in the size, shape and distribution of the interstitial nanovoids [57, 58]. Furthermore, thermal annealing has been reported to increase the medium-range order in amorphous tantala-based films [59–61]. The release of Argon embedded in the film at deposition (an undesired effect of IBS) can be also at play [62], though likely greatly attenuated by annealing in atmospheric conditions [22]. Another mechanism that has been proposed to explain the enhancement of the coating properties during annealing in air is the removal of a slight oxygen deficit, that has been reported in the as-deposited coating [63]. Untangling and tracking the above mechanisms at work during annealing by means of optical measurements solely appears to be an arduous and probably inaccessible task. In the following, we indicate

how the reported real-time data can provide suggestions to promote a further enhancement of the coatings properties by means of a different choice of annealing parameters.

During the heating ramp (left panel in figure 5) we note that the variations begin once the temperature of the coating is raised above the deposition temperature, which in this case is much lower than the maximum annealing temperature. We recall that the deposition temperature is a key parameter to define the 'initial' state of the coating, including the stress [17, 64–66]. A higher deposition temperature might lead to coatings with a more relaxed initial state and enhance their medium-range order in a way which is more efficient that the one accessible via postdeposition annealing [67]. Therefore, increasing the deposition temperature is desirable in coatings for GWD applications.

Once the coating reaches the maximum-temperature plateau, the evolution of its observed properties is still underway even after 10 h. This clearly indicates that the current annealing protocol leaves room for further modifications in the coatings properties, which can be probed for example by increasing the time duration of the plateau. A further element of analysis is provided by the Urbach energy, a parameter whose decrease has been correlated to an increase in the medium-range order of the amorphous coating structure [68]. The Urbach energy depends not only on the structural and compositional ordering of the material, but also on its thermal disorder [69]. Therefore during the heating ramp, the variations in the Urbach energy are due not only to the structural modifications in the coating, but also to the increasing temperature. Disentangling the structural contribution in this case would require new experiments which could be considered in future works. On the other hand, any variations in the Urbach energy recorded during the high-temperature plateau, when the temperature is constant, can be directly related to the structural and compositional order of the coating. In this work, we found that the Urbach energy of the coating during the high-temperature plateau decreased by 4 ± 1 meV, while we previously reported that the overall decrease of the Urbach energy after the whole annealing process is around 45 meV [36]. This result further proves that most of the variations in the titania-tantala coating occur during the heating ramp, with comparatively smaller changes recorded during the high-temperature plateau. In summary, the real-time data reported in this work suggest the current annealing protocol for GWD mirrors leaves room for further modifications in the properties of the titania-tantala coatings, which might be achieved for instance by increasing the time duration of the 500 °C plateau, while monitoring the variations of Urbach energy at constant temperature.

4. Concluding remarks and perspectives

By applying real-time, *in situ* SE measurements we have tracked the refractive index and thickness of an amorphous, mixed titania-tantala coating during an entire annealing cycle. The coating material and the parameters of the annealing process have been chosen to test those employed in current GWD mirrors. Results indicate that the largest variations, in the range of 1% or more, occur during the heating ramp from room temperature to the maximum temperature of 500 °C. Variations start occurring above $\sim$200 °C, just above the deposition temperature. A comparatively smaller evolution of the optical thickness, in the range of 0.1%, is observed during the following 10-h long plateau at 500 °C. The evolution of the tracked properties is still well underway upon reaching the maximum temperature, and also at the end of the 10-h plateau, indicating that the current annealing protocol leaves room for further evolution of the titania-tantala coatings properties, possibly leading to an enhancement of their performance for GWD applications. Indeed, the results of this work suggest increasing the maximum annealing temperature and the time duration of the high-temperature plateau. The method described

here could be usefully employed to test new annealing protocols involving rates, durations and maximum temperature. The upper boundary in the choice of the latter remains set by the onset of crystallization, which must be avoided anyway.

This work also indicates that the evolution of the tracked coating properties starts slightly above the deposition temperature, with a maximum recorded variation rate around 300 °C. Raising the deposition temperature at least to up that value might further promote the medium-range order in the coating, which is known to be beneficial for GWD applications. A different deposition temperature would most likely determine a different evolution in the coating properties during the annealing. In this respect, a promising strategy for enhancing the properties of optical coatings could be to consider deposition and annealing as two complementary processes to be optimized in synergy.

The real-time optical analysis during the annealing can be of use in the ongoing research effort to find, screen and validate new materials and even new designs [70, 71] for GWD mirrors. Nowadays, titania-Germania coating is being intensively studied to replace titania-tantala in future upgrades of GWD mirrors due to its low thermal noise [17]. Titania-Germania—or any other choice of coating material—must be annealed after deposition and the annealing protocol has to be optimized. The task of finding the optimal parameters, which are expected to change from one material to the other, could be greatly helped by real-time investigation tools, such as the one reported in this paper. In this respect, we already initiated an experimental campaign applying the real-time SE analysis to different amorphous mixed oxide coatings and new annealing protocols, which we aim to present in future dedicated works.

Data availability statement

All data that support the findings of this study are included within the article (and any supplementary files). Tabulated data of the SE measurements as a function of time and temperature can be found at the OSF online repository [72].

Acknowledgments

We gratefully acknowledge the Project Einstein Telescope Infrastructure Consortium (ETIC) (IR0000004)-MUR call n. 3264 PNRR, Miss. 4-Comp. 2, Line 3.1. We thank the Virgo Coating R&D collaboration for fruitful discussions. We thank Dr Francesco Bisio for support in the setting of the heating cell and the development of related experimental methods. We acknowledge the support of Davide Odino for AFM measurements.

Conflict of interest

There are no conflicts of interest to declare.

ORCID iDs

Stefano Colace https://orcid.org/0009-0007-9429-1847
Shima Samandari https://orcid.org/0009-0002-8571-379X
Massimo Granata https://orcid.org/0000-0003-3275-1186

Alex Amato https://orcid.org/0000-0001-9557-651X
Michael Caminale https://orcid.org/0000-0002-2209-1818
Gianluca Gemme https://orcid.org/0000-0002-1127-7406
Maurizio Canepa https://orcid.org/0000-0002-5148-1233
Michele Magnozzi https://orcid.org/0000-0003-4512-8430

References

[1] He X, Wu J, Li X, Gao X, Gan X and Zhao L 2009 Effects of the post-annealing ambience on the microstructure and optical properties of tantalum oxide films prepared by pulsed laser deposition *J. Alloys Compd.* **478** 453–7
[2] Sertel T, Sonmez N A, Cetin S S and Ozcelik S 2019 Influences of annealing temperature on anti-reflective performance of amorphous Ta_2O_5 thin films *Ceram. Int.* **45** 11–18
[3] Khan S B, Zhang Z and Lee S L 2020 Annealing influence on optical performance of HfO_2 thin films *J. Alloys Compd.* **816** 152552
[4] Jin Y, Bond C W, Leonard R L, Liu Y, Johnson J A and Petford-Long A K 2021 The effect of annealing on optical transmittance and structure of ZLANI fluorozirconate glass thin films *Micron* **140** 102977
[5] Title A M, Pope T P and Andelin J P 1974 Drift in interference filters. Part 1 *Appl. Opt.* **13** 2675–9
[6] Hass G 1952 Preparation, properties and optical applications of thin films of titanium dioxide *Vacuum* **2** 331–45
[7] Brown J T 2004 Center wavelength shift dependence on substrate coefficient of thermal expansion for optical thin-film interference filters deposited by ion-beam sputtering *Appl. Opt.* **43** 4506–11
[8] Stenzel O 2014 *Optical Coatings. Material Aspects in Theory and Practice* (Springer)
[9] Granata M *et al* 2016 Mechanical loss in state-of-the-art amorphous optical coatings *Phys. Rev.* D **93** 012007
[10] Harry G and Billingsley G *Advanced Interferometric Gravitational-Wave Detectors* ch 19, pp 521–54 Ch 19
[11] Granata M *et al* 2020 Progress in the measurement and reduction of thermal noise in optical coatings for gravitational-wave detectors *Appl. Opt.* **59** A229
[12] Granata M *et al* 2020 Amorphous optical coatings of present gravitational-wave interferometers *Class. Quantum Grav.* **37** 095004
[13] Durante O *et al* 2023 Investigation of crystallization in nanolayered TiO_2-based superlattices *Surf. Interfaces* **41** 103309
[14] Anghinolfi L, Prato M, Chtanov A, Gross M, Chincarini A, Neri M, Gemme G and Canepa M 2013 Optical properties of uniform, porous, amorphous Ta_2O_5 coatings on silica: temperature effects *J. Phys. D: Appl. Phys.* **46** 455301
[15] Amato A *et al* 2018 High-reflection coatings for gravitational-wave detectors: state of the art and future developments *J. Phys.: Conf. Ser.* **957** 012006
[16] Durante O *et al* 2021 Emergence and evolution of crystallization in TiO_2 thin films: a structural and morphological study *Nanomaterials* **11** 1409
[17] Vajente G *et al* 2021 Low mechanical loss TiO_2GeO_2 coatings for reduced thermal noise in gravitational wave interferometers *Phys. Rev. Lett.* **127** 071101
[18] Fazio M A, Vajente G, Yang L, Ananyeva A and Menoni C S 2022 Comprehensive study of amorphous metal oxide and Ta_2O_5-based mixed oxide coatings for gravitational-wave detectors *Phys. Rev.* D **105** 102008
[19] Favaro G *et al* 2022 Measurement and simulation of mechanical and optical properties of sputtered amorphous SiC coatings *Phys. Rev. Appl.* **18** 044030
[20] Todorow B, von Bogen O and Kanellis S 2000 Apparatus for real-time observations of the annealing process of metallic glasses *J. Magn. Magn.* **215–216** 499–502
[21] Abernathy M R, Hough J, Martin I W, Rowan S, Oyen M, Linn C and Faller J E 2014 Investigation of the Young's modulus and thermal expansion of amorphous titania-doped tantala films *Appl. Opt.* **53** 3196–202
[22] Paolone A *et al* 2021 Effects of the annealing of amorphous Ta_2O_5 coatings produced by ion beam sputtering concerning the effusion of argon and the chemical composition *J. Non-Cryst. Solids* **557** 120651

[23] Rezac M, Martinez D, Gleckl A and Smith J R 2023 Imaging scatterometer for observing in situ changes to optical coatings during air annealing *Appl. Opt.* **62** B97–B103
[24] Harry G M *et al* 2007 Titania-doped tantala/silica coatings for gravitational-wave detection *Class. Quantum Grav.* **24** 405–15
[25] Pinard L *et al* 2017 Mirrors used in the LIGO interferometers for first detection of gravitational waves *Appl. Opt.* **56** C11
[26] Flaminio R, Franc J, Michel C, Morgado N, Pinard L and Sassolas B 2010 A study of coating mechanical and optical losses in view of reducing mirror thermal noise in gravitational wave detectors *Class. Quantum Grav.* **27** 084030
[27] Magnozzi M, Bisio F and Canepa M 2017 Solid-state dewetting of thin Au films studied with real-time, in situ spectroscopic ellipsometry *Appl. Surf. Sci.* **421** 651–5
[28] Magnozzi M, Haghighian N, Miseikis V, Cavalleri O, Coletti C, Bisio F and Canepa M 2017 Fast detection of water nanopockets underneath wet-transferred graphene *Carbon* **118** 208–14
[29] Magnozzi M *et al* 2018 Optical properties of amorphous SiO_2-TiO_2 multi-nanolayered coatings for 1064-nm mirror technology *Opt. Mater.* **75** 94–101
[30] Amato A *et al* 2019 Optical properties of high-quality oxide coating materials used in gravitational-wave advanced detectors *J. Phys.: Mater.* **2** 035004
[31] Magnozzi M, Ferrera M, Mattera L, Canepa M and Bisio F 2019 Plasmonics of Au nanoparticles in a hot thermodynamic bath *Nanoscale* **11** 1140–6
[32] Magnozzi M, Brasse Y, König T A F, Bisio F, Bittrich E, Fery A and Canepa M 2020 Plasmonics of Au/polymer core/shell nanocomposites for thermoresponsive hybrid metasurfaces *ACS Appl. Nano Mater.* **3** 1674–82
[33] Collaboration T V *et al* 2004 The VIRGO large mirrors: a challenge for low loss coatings *Class. Quantum Grav.* **21** S935–45
[34] Tompkins H and Hilfiker J 2016 *Spectroscopic Ellipsometry: Practical Applications to Thin Film Characterization* (Momentum Press)
[35] Synowicki R A 2008 Suppression of backside reflections from transparent substrates *Phys. Status Solidi* C **5** 1085–8
[36] Amato A, Magnozzi M, Shcheblanov N, Lemaitre A, Cagnoli G, Granata M, Michel C, Gemme G, Pinard L and Canepa M 2023 Enhancing titania-tantala amorphous materials as high-index layers in bragg reflectors of gravitational-wave detectors *ACS Appl. Opt. Mater.* **1** 395–402
[37] Fujiwara H 2007 *Spectroscopic Ellipsometry* (Wiley)
[38] Magnozzi M, Ferrera M, Canepa M and Bisio F 2019 Monitoring the solid-state dewetting of densely packed arrays of Au nanoparticles *J. Phys.: Conf. Ser.* **1226** 012014
[39] Magnozzi M, Bisio F, Gemme G, Granata M, Michel C, Pinard L and Canepa M 2023 Detecting ultrathin ice on materials for optical coatings at cryogenic temperatures *J. Phys. D: Appl. Phys.* **56** 475105
[40] Nečas D and Klapetek P 2012 Gwyddion: an open-source software for SPM data analysis *Cent. Eur. J. Phys.* **10** 181–8
[41] Li H H 1980 Refractive index of silicon and germanium and its wavelength and temperature derivatives *J. Phys. Chem. Ref. Data* **9** 561–658
[42] Lautenschlager P, Garriga M, Vina L and Cardona M 1987 Temperature dependence of the dielectric function and interband critical points in silicon *Phys. Rev.* B **36** 4821–30
[43] Vuye G, Fisson S, Nguyen Van V, Wang Y, Rivory J and Abelés F 1993 Temperature dependence of the dielectric function of silicon using in situ spectroscopic ellipsometry *Thin Solid Films* **233** 166–70
[44] Jellison G E and Modine F A 1994 Optical functions of silicon at elevated temperatures *J. Appl. Phys.* **76** 3758–61
[45] Šik J, Hora J and Humlíček J 1998 Optical functions of silicon at high temperatures *J. Appl. Phys.* **84** 6291–8
[46] Herzinger C and Johs B 1998 Dielectric function parametric model, and methods of use *U.S. Patent* 5796983
[47] ET Editorial Team Design report update 2020 for the Einstein Telescope. ET public document, Technical Documentation System number: ET-0007B-20 2020
[48] Amato A, Terreni S, Granata M, Michel C, Pinard L, Gemme G, Canepa M and Cagnoli G 2019 Effect of heating treatment and mixture on optical properties of coating materials used in gravitational-wave detectors *J. Vac. Sci. Technol.* B **37** 062913

[49] Ogin G H 2013 Measurement of thermo-optic properties of thin film dielectric coatings *PhD Thesis* California Institute of Technology Pasadena, California (USA)
[50] Macleod A 2018 *Thin-Film Optical Filters* 5th edn (CRC Press, Taylor & Francis Group)
[51] Bischoff M, Nowitzki T, Voß O, Wilbrandt S and Stenzel O 2014 Postdeposition treatment of IBS coatings for UV applications with optimized thin-film stress properties *Appl. Opt.* **53** A212–20
[52] Windischmann H 1992 Intrinsic stress in sputter-deposited thin films *Crit. Rev. Solid State Mater. Sci.* **17** 547–96
[53] Bassiri R, Borisenko K B, Cockayne D J H, Hough J, MacLaren I and Rowan S 2011 Probing the atomic structure of amorphous Ta_2O_5 coatings *Appl. Phys. Lett.* **98** 031904
[54] Bassiri R *et al* 2015 Order within disorder: the atomic structure of ion-beam sputtered amorphous tantala (a-Ta_2O_5) *APL Mater.* **3** 036103
[55] Bassiri R *et al* 2016 Order, disorder and mixing: The atomic structure of amorphous mixtures of titania and tantala *J. Non-Cryst. Solids* **438** 59–66
[56] Damart T, Coillet E, Tanguy A and Rodney D 2016 Numerical study of the structural and vibrational properties of amorphous Ta_2O_5 and TiO_2-doped Ta_2O_5 *J. Appl. Phys.* **119** 175106
[57] Prasai K *et al* 2019 High precision detection of change in intermediate range order of amorphous zirconia-doped tantala thin films due to annealing *Phys. Rev. Lett.* **123** 045501
[58] Thapa R, Prasai K, Bassiri R, Fejer M M and Drabold D A 2022 Realistic computer models of amorphous ZrO_2 : Ta_2O_5 structural, optical and vibrational properties *Phys. Rev.* B **105** 224207
[59] Hart M J, Bassiri R, Borisenko K B, Véron M, Rauch E F, Martin I W, Rowan S, Fejer M M and MacLaren I 2016 Medium range structural order in amorphous tantala spatially resolved with changes to atomic structure by thermal annealing *J. Non-Cryst. Solids* **438** 10–17
[60] Shyam B, Stone K H, Bassiri R, Fejer M M, Toney M F and Mehta A 2016 Measurement and modeling of short and medium range order in amorphous Ta_2O_5 thin films *Sci. Rep.* **6** 32170
[61] Mishkin A, Jiang J, Zhang R, Cheng H-P, Prasai K, Bassiri R and Fejer M 2023 Hidden structure in the medium-range order of amorphous zirconia-tantala films *Phys. Rev.* B **108** 054103
[62] Paolone A *et al* 2022 Argon and other defects in amorphous SiO_2 coatings for gravitational-wave detectors *Coatings* **12** 1001
[63] Kim N and Stebbins J F 2013 Effects of annealing on the structure of ion beam sputtered amorphous tantalum oxide: Oxygen-17 NMR spectra and relaxation times *J. Non-Cryst. Solids* **378** 158–62
[64] Parisi G and Sciortino F 2013 Flying to the bottom *Nat. Mater.* **12** 94–95
[65] Vajente G *et al* 2018 Effect of elevated substrate temperature deposition on the mechanical losses in tantala thin film coatings *Class. Quantum Grav.* **35** 075001
[66] Prasai K *et al* 2023 Effects of elevated-temperature deposition on the atomic structure of amorphous Ta_2O_5 films *APL Mater.* **11** 121112
[67] Yang L *et al* 2021 Enhanced medium-range order in vapor-deposited germania glasses at elevated temperatures *Sci. Adv.* **7** eabh1117
[68] Amato A, Terreni S, Granata M, Michel C, Sassolas B, Pinard L, Canepa M and Cagnoli G 2020 Observation of a correlation between internal friction and urbach energy in amorphous oxides thin films *Sci. Rep.* **10** 1670
[69] Studenyak I and Kranjcec M M K 2014 Urbach rule in solid state physics *Int. J. Opt. Appl.* **4** 76
[70] Craig K *et al* 2019 Mirror coating solution for the cryogenic einstein telescope *Phys. Rev. Lett.* **122** 231102
[71] Pierro V *et al* 2021 Ternary quarter wavelength coatings for gravitational wave detector mirrors: design optimization via exhaustive search *Phys. Rev. Res.* **3** 023172
[72] Magnozzi M 2024 Monitoring the evolution of optical coatings during thermal annealing (available at: https://osf.io/ahby9/)